Polarization Control by Using Anisotropic 3-D Chiral Structures

Menglin L. N. Chen, *Student Member, IEEE*, Li Jun Jiang, *Senior Member, IEEE*, Wei E. I. Sha, *Member, IEEE*, Wallace C. H. Choy, *Senior Member, IEEE*, and Tatsuo Itoh, *Life Fellow, IEEE*

***Abstract*— Due to the mirror symmetry breaking, chiral structures show fantastic electromagnetic (EM) properties involving negative refraction, giant optical activity, circular dichroism and asymmetric transmission. Aligned electric and magnetic dipoles excited in chiral structures contribute to the extraordinary properties. However, the chiral structures that exhibit *n*-fold rotational symmetry show a limited tunability of the chirality. In this paper, we propose a compact, light, and highly tunable anisotropic chiral structure to overcome this limitation and realize a linear-to-circular polarization conversion. The anisotropy is due to simultaneous excitations of two different pairs of aligned electric and magnetic dipoles. The 3-D omega-shaped structure, etched on two sides of one printed circuit board (PCB) with connecting metallic vias, achieves 60% of linear-to-circular conversion (transmission) efficiency at the operating frequency of 9.2 GHz. The desired 90° phase shift between the two orthogonal linear polarizations is not only from the chirality but also from the anisotropic chiral response slightly off the resonance. The work enables elegant and practical polarization control of EM waves.**

***Index Terms*— Chiral structure, circular polarizer, polarization control.**

I. Introduction

CHIRAL structures are composed of particles that cannot be superimposed on their mirror images. The asymmetric geometry of a chiral particle results in the cross coupling between electric f eld and magnetic field Therefore, a chiral medium is also known as a bi-isotropic medium if it has identical electromagnetic (EM) responses in all directions [1]. Chiral media can be found in nature. However, the chirality is usually very weak. Chirality can be enhanced in artificia materials. With strong chirality, it could be easier to realize the negative refractive index in chiral structure compared to the conventional negative-index metamaterial composed of split-ring resonators (SRRs) and metallic wires [2]. Besides the negative refractive index, chiral structure shows other interesting features like giant optical activity, circular dichroism and asymmetric transmission [3]–[5].

Various man-made chiral “molecules” have been analyzed and the corresponding parameter retrieval method has been studied [6]. Generally, chiral structure can be classif ed into two groups: planar chiral structure and 3-D chiral structure. Planar chiral structures like rosettes [7], [8] and cross wires [9] are easy to fabricate. They exhibit giant optical activity and negative refractive index at different frequency bands for right circularly polarized (RCP) and left circularly polarized (LCP) waves. Typical prototypes of the 3-D chiral structure originate from helical geometry, such as chiral SRR [10], omega-shaped particle [11], [12], and cranks [13]. These 3-D chiral structures have been well designed so that they can be fabricated as planar ones on printed circuit boards (PCBs). Additionally, the supercell technique has been applied in the U-shaped chiral structures [14], [15] to gain better tunability. Among all the chiral structures, the planar ones usually present n-fold rotational symmetry. The rotational symmetry makes the planar chiral structure insensitive to the polarization direction of normal incident wave and sets up limitations to its control of polarization properties. Unlike the planar chiral structure, the 3-D chiral structure is usually sensitive to the polarization state of incident wave and allows for a fl xible control of polarization. Therefore, the polarization conversion such as linear-to-circular conversion can be realized by the 3-D chiral structure.

In this paper, we explore the polarization control capability of a 3-D omega-shaped chiral structure comprehensively. Even though a similar structure has been proposed in [12] and its origin of chirality is explained by a resonant inductor-capacitor (LC) circuit, we explore the physical origin of the chirality in our proposed 3-D omega-shaped structure based on the induced EM f elds. And then, we offer a new physical insight to its excitation condition and polarization responses with varying geometries. Here, we f nd the 3-D omega-shaped chiral structure shows a great capability to manipulate the polarization state of EM waves. First, we show the polarization state of the transmitted EM wave by the chiral structure can be tuned in a wide range by twisting the arms of the chiral particle. Second, we theoretically and experimentally demonstrate an anisotropic omega-shaped chiral structure designed as a circular polarizer. Compared to conventional polarizers, the chiral polarizer has an ultra compact volume. Third, we design a uniaxial omega-shaped chiral structure. It generates giant optical activity which is not sensitive to the polarization state of normal incident wave and shows advantages over other

Manuscript received January 20, 2016; revised May 15, 2016; accepted July 26, 2016. Date of publication August 16, 2016; date of current version October 27, 2016. This work was supported in part by the Research Grants Council of Hong Kong under Grant GRF 716713, Grant GRF 17207114, and Grant GRF 17210815, in part by NSFC under Grant 61271158, in part by Hong Kong under Grant ITP/045/14LP, in part by Hong Kong UGC under Grant AoE/PC04/08, in part by the Collaborative Research Fund from the Research Grants Council of Hong Kong, under Grant C7045-14E, and in part by CAS-Croucher Funding Scheme for Joint Laboratories under Grant CAS14601.

M. L. N. Chen, L. J. Jiang, W. E. I. Sha, and W. C. H. Choy are with the Department of Electrical and Electronic Engineering, The University of Hong Kong, Hong Kong (e-mail: menglin@connect.hku.hk; jianglj@hku.hk; wsha@eee.hku.hk; chchoy@eee.hku.hk).

T. Itoh is with the Electrical Engineering Department, University of California Los Angeles, Los Angeles, CA 90095 USA (e-mail: itoh@ee.ucla.edu).

Color versions of one or more of the f gures in this paper are available online at http://ieeexplore.ieee.org.

Digital Object Identifie 10.1109/TAP.2016.2600758

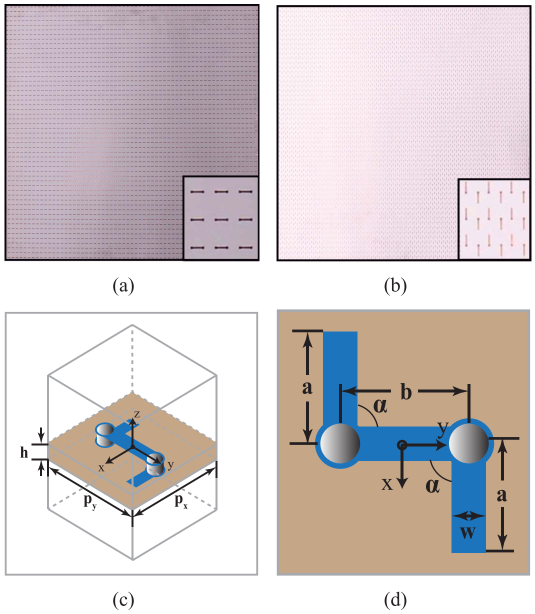

Fig. 1. Illustration of the chiral structure. (a) Photograph of the top layer of a fabricated sample slab. (b) Photograph of the bottom layer of the fabricated sample slab. (c) Schematic of the twisted omega-shaped chiral unit cell with the periodicity along the x- and y-directions. (d) Top view of the chiral unit cell. Lattice constants are denoted by p_x and p_y, respectively. The thickness of dielectric substrate is h, which is the same as the height of the two vias of the chiral unit cell. Arm lengths of the particle are a and b at the bottom and the top layers, respectively. The angle between the arm at the top layer and that at the bottom layer is represented by α.

uniaxial 3-D chiral structures arranged in the Bravais lattice in terms of the complexity of fabrication [10]. All our proposed chiral structures can be conveniently fabricated using the PCB technique.

II. Origin of Chirality

In this section, we discuss the origin of the chirality of the 3-D omega-shaped chiral structure by analyzing the directions of the induced EM f elds, which has not been published before, according to our best knowledge.

A. Electric- And Magnetic-Dipole Pairs

The proposed chiral structure is shown in Fig. 1. Fig. 1(c) and (d) shows the schematic pattern of one chiral particle at different viewing angles. The chiral particle can be simply seen as a twisted conducting wire in 3-D domain. It consists of fi e segments: the two vertical segments (vias) connect the two horizontal segments (wires) and one vertical segment (wire), which are placed at the bottom and top of the substrate, respectively. This geometry has complete symmetry breaking along the x-, y-, and z-directions, indicating the strong chirality.

The chiral particle has a total length of l, where $l = 2a + b + 2h$. a and b are the lengths of the segments shown in Fig. 1(d) and h is the height of the vertical segments. The f rst (fundamental) resonance of the chiral particle is the half-wavelength resonance, which should satisfy $l = \lambda_{\text{eff}}/2$, where λ_{eff} is the effective wavelength. In the following analysis, we will only consider the half-wavelength resonance to achieve a compact design. Under this condition, the periodic length (lattice constant) of the chiral structure is much smaller than the incident wavelength, so that only the zeroth-order diffraction exists. Current direction and charge accumulation are drawn in Fig. 2(a). Charges are accumulated at the two ends of the chiral particle, forming an electric dipole in the xoy plane. The electric dipole has both x- and y-components. By looking at the x-direction as shown in Fig. 2(b), a current loop can be formed and it generates a magnetic dipole pointing at the x-direction. The magnetic dipole is aligned with the x-component of the electric dipole. Besides this electric- and magnetic-dipole pair, when we look at the y-direction, another pair aligned with the y-direction can be found as illustrated in Fig. 2(c). It is well known that chirality of a medium arises from the coupled electric and magnetic f elds. In the proposed chiral particle, there are two pairs of electric and magnetic dipoles. This special conf guration facilitates the tunable chirality, because the strengths of both x- and y-components of the electric and magnetic dipoles can be adjusted by changing the angle α and segment lengths [see Fig. 1(d)].

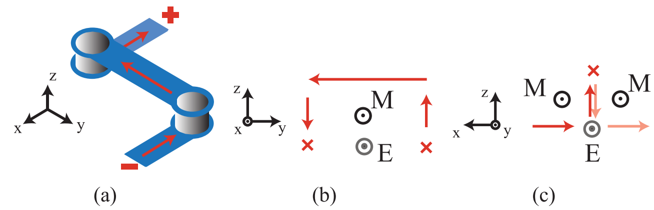

Fig. 2. Illustration of fundamental mode of the proposed omega-shaped chiral particle. The current direction (red arrow) and the induced magnetic and electric dipoles are observed at different viewing angles. (a) 3-D view of the chiral particle resonating at the fundamental (half-wavelength) mode. (b) Current direction viewed from the x-axis and the induced electric- and magnetic-dipole pair along the x-direction. (c) Current direction viewed from the y-axis and the induced electric- and magnetic-dipole pair along the y-direction.

B. Excitation

Excitation condition for the fundamental resonant mode of the proposed chiral particle is explored. One unit cell in a cuboid box with two sets of periodic boundaries and one set of Floquet port is simulated in Ansoft HFSS as shown in Fig. 3.

When the periodicity is along the x- and y-axes, i.e., periodic boundary conditions are applied at the transverse xoy plane while two f oquet ports are assigned on the top and bottom boundaries along the z-direction, the fundamental mode can be successfully excited. The reason for this effective excitation can be explained using mode matching theory [16]. As discussed, we have the x- and y-components for both electric and magnetic dipoles. When the plane wave propagates along z-axis, no matter what the polarization direction is, the incident electric (magnetic) f eld could be aligned with the x- or y-component of the induced electric (magnetic) dipole. As a result, the mode conversion occurs between the plane wave (propagating in free space) and the fundamental standing wave (supported in the chiral particle). Due to the anisotropy in this chiral particle, the spatial overlap between the plane wave and the fundamental mode highly depends on the polarization direction of the plane wave. Therefore, although the chiral

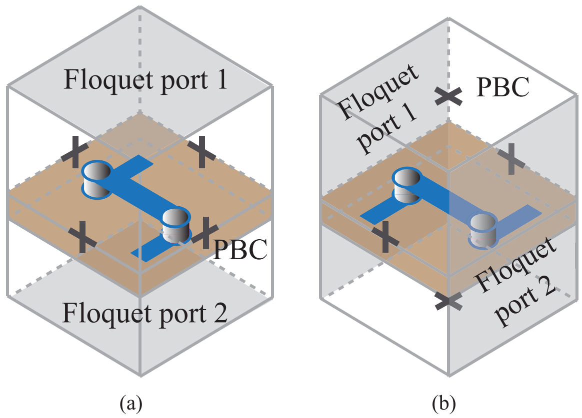

Fig. 3. Simulation configur tions in HFSS. (a) Excitation from top with two pairs of periodic boundaries at the four lateral faces. (b) Excitation from the side with one pair of periodic boundaries on the two lateral faces and the other pair on the top and bottom faces. Here, ++++ stands for the periodic boundary.

particle can be excited under either x or y polarized incident f eld, the transmission and ref ection responses under the two cases of incidence will be different.

If the periodicity is along the z- and x-axes, the fundamental mode cannot be excited due to the polarization misalignment. When the wave impinging from the lateral side is x polarized, the vertical magnetic fiel is not aligned with the magnetic dipole, since there is no z-component of the magnetic dipole. When the wave is polarized at the z-direction, the electric dipole at the xoy plane cannot be aligned with the incident electric f eld. Similarly, the fundamental mode cannot be excited when the periodicity is along the z- and y-axes. In conclusion, the proposed chiral particle can only be signif cantly excited at the normal incidence along the z-axis.

From above analyses, the chiral structure could be implemented using the PCB technique with a substrate inserted into the xoy plane. Moreover, it is important to emphasize that the induced electric- and magnetic-dipole pairs are parallel to the substrate plane, which is quite different from the 3-D chiral particle reported in [10]. The photograph of a fabricated chiral slab is shown in Fig. 1(a) and (b).

III. Polarization Control

Assuming a plane wave propagates along the z-direction and penetrates a chiral medium, the incident and transmitted electric f elds can be decomposed into the two linear x- and y-components

$$\mathbf{E}_i(\mathbf{r},t) = \begin{pmatrix} i_x \\ i_y \end{pmatrix} e^{i(kz-\omega t)}, \quad \mathbf{E}_t(\mathbf{r},t) = \begin{pmatrix} t_x \\ t_y \end{pmatrix} e^{i(kz-\omega t)} \tag{1}$$

where ω is the wave frequency, k is the wave number, and the complex amplitudes i_x, i_y and t_x, t_y represent the polarization states of the incident and transmitted waves.

To model a chiral particle, the transmission matrix T that connects the polarization state of the transmitted wave to that of the incident wave is constructed in the linear basis [17]

$$\begin{pmatrix} t_x \\ t_y \end{pmatrix} = \begin{pmatrix} T_{xx} & T_{xy} \\ T_{yx} & T_{yy} \end{pmatrix} \begin{pmatrix} i_x \\ i_y \end{pmatrix} = T_{\text{lin}} \begin{pmatrix} i_x \\ i_y \end{pmatrix} \tag{2}$$

where the f rst and second subscripts of T denote the polarization states of the transmitted and incident waves, respectively. Then, the transmission matrix in the circular basis can be obtained from that in the linear basis (see (3), shown at the bottom of this page), where $+$ and $-$ represent the RCP and LCP waves.

For a bi-isotropic chiral medium, the the coupling effect between the electric and magnetic field leads to two different wave vectors for plane wave with two eigenvectors corresponding to the RCP wave and LCP wave, respectively. Thus, the polarization state of incident wave changes through the chiral medium. Polarization responses of the chiral medium are characterized by the optical activity and circular dichroism. Optical activity is the polarization rotation phenomenon for a linearly polarized incident wave. Mathematically, it is represented by the azimuthal rotation angle θ. Circular dichroism characterizes the polarization transition of an incident wave, such as the change of a polarization state from linear to elliptical. The circular dichroism is measured by the ellipticity η. θ and η can be calculated by

$$\theta = \frac{1}{2}[\arg(T_{++}) - \arg(T_{--})] \tag{4a}$$

$$\eta = \frac{1}{2}\sin^{-1}\left(\frac{|T_{++}|^2 - |T_{--}|^2}{|T_{++}|^2 + |T_{--}|^2}\right). \tag{4b}$$

For planar chiral structures, typically having fourfold (C_4) rotational symmetry, the transmission matrix has the following form:

$$T_{\text{lin}}^{C_4} = \begin{pmatrix} T_{xx} & T_{xy} \\ -T_{xy} & T_{xx} \end{pmatrix} \tag{5a}$$

$$T_{\text{circ}}^{C_4} = \begin{pmatrix} T_{xx} + iT_{xy} & 0 \\ 0 & T_{xx} - iT_{xy} \end{pmatrix}. \tag{5b}$$

It can be seen that the transmission coefficient in linear basis are not independent but show specif c relations. The resultant transmission matrix in circular basis is diagonal.

Through our design, optical activity and circular dichroism can be engineered by tailoring the mutual coupling between the electric and magnetic field . Since there are many degrees of freedom for the proposed chiral particle, namely the segment lengths a and b, the height of the vias h, and the twisting angle α [see Fig. 1(d)], the azimuthal rotation angle and ellipticity could be tuned over a large range. Here, we tune the chiral property by modifying α with counterclockwise rotation of the two arms on the bottom layer as illustrated in Fig. 4(a).

The angle α greatly infl ences the direction and strength of the induced electric and magnetic dipoles. For example, when α increases in the f rst two quadrants, the separation between the two ends of the chiral particle increases. Consequently,

$$T_{\text{circ}} = \begin{pmatrix} T_{++} & T_{+-} \\ T_{-+} & T_{--} \end{pmatrix} = \frac{1}{2}\begin{pmatrix} (T_{xx}+T_{yy}) + i(T_{xy}-T_{yx}) & (T_{xx}-T_{yy}) - i(T_{xy}+T_{yx}) \\ (T_{xx}-T_{yy}) + i(T_{xy}+T_{yx}) & (T_{xx}+T_{yy}) - i(T_{xy}-T_{yx}) \end{pmatrix} \tag{3}$$

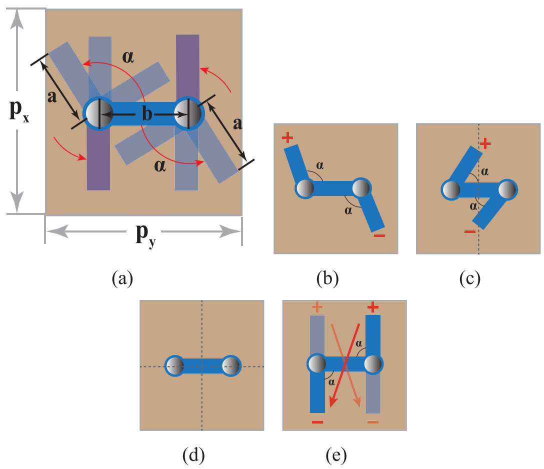

Fig. 4. Schematic of the chiral unit cell with different configuration of twisting angle α. The signs of accumulated charges at the two ends of the chiral particle are denoted under the illumination of the x polarized wave. (a) Rotation pattern of the two arms at the horizontal plane. (b) $\alpha > 90°$. (c) $\alpha < 90°$. (d) $\alpha = 0°$. (e) $\alpha = -90°$ (solid blue color) and $\alpha = 90°$ (semi-transparent blue color). Arm lengths are set to be $a = b = 3$ mm. The length of the vertical vias is $h = 1.6$ mm. The square unit cell occupies 8×8 mm.

the strength of the electric dipole decreases, and the coupling between the electric and magnetic fiel s is weakened. Chirality depending on the coupling effect will be reduced in Fig. 4(b) compared with Fig. 4(c). Moreover, α also determines the direction of electric and magnetic dipoles. For example, in Fig. 4(c), no y-component of the induced electric dipole can be found. In Fig. 4(d), when $\alpha = 0$, the direction of the induced electric dipole only has the y-component; and the magnetic dipole only has the x-component. In this case, no aligned electric- and magnetic-dipole pair can be generated, resulting in the vanishing chirality. Additionally, when α goes to negative values, for instance $-90°$ in Fig. 4(e), compared to the case of $\alpha = 90°$, the strengths of the induced f elds are identical, but the direction of the y-component of the induced electric dipole is reversed. Thus, the cross-transmission coeffi cients T_{xy} and T_{yx} have opposite signs for the cases of $\alpha = 90°$ and $\alpha = -90°$. Mathematically, we have

$$T_{\text{lin}}^{\alpha} = \begin{pmatrix} T_{xx} & T_{xy} \\ T_{yx} & T_{yy} \end{pmatrix}, \quad T_{\text{lin}}^{-\alpha} = \begin{pmatrix} T_{xx} & -T_{xy} \\ -T_{yx} & T_{yy} \end{pmatrix} \tag{6}$$

$$T_{\text{circ}}^{\alpha} = \begin{pmatrix} T_{++} & T_{+-} \\ T_{-+} & T_{--} \end{pmatrix}, \quad T_{\text{circ}}^{-\alpha} = \begin{pmatrix} T_{--} & T_{-+} \\ T_{+-} & T_{++} \end{pmatrix}. \tag{7}$$

We can derive that $\theta^{\alpha} = -\theta^{-\alpha}$ and $\eta^{\alpha} = -\eta^{-\alpha}$.

For simplicity, no dielectric substrate is considered in the simulation, which will not affect the conclusion to be made. The azimuthal rotation angle and ellipticity for the cases with different twisting angle α are plotted in Fig. 5. As expected, the azimuthal rotation angle and ellipticity are zeros in the whole frequency band when $\alpha = 0$ (the green-star curves). When α is not equal to zero, the peak values of both θ and η increase as α decreases. Meanwhile, both θ and η have opposite signs for $\alpha = 90°$ and $\alpha = -90°$. All the simulation results are in good agreement with above theoretical analyses. It is worthy of noticing that the resonant frequency (i.e., the frequency when θ is zero) of the chiral particle is shifted to a lower frequency

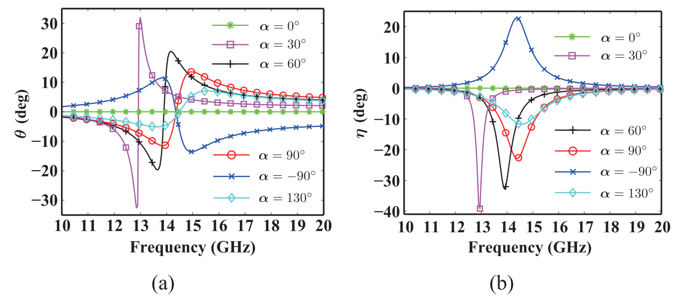

Fig. 5. Polarization responses of the chiral structure with the varying twisting angle α. The other parameters are the same as described in Fig. 4 and no dielectric substrate is adopted. (a) Azimuthal rotation angle. (b) Ellipticity.

as α decreases. This can be explained by the influenc of α on the mutual coupling between the electric and magnetic f elds. Stronger coupling between the electric and magnetic f elds can be regarded as extra LC loads of the chiral particle leading to a lower resonant frequency. When α is larger than 90°, the coupling of the electric and magnetic f elds has already become very weak so that its influenc becomes less obvious. Therefore, we can notice that the difference between the resonant frequencies when $\alpha = 60°$ and $\alpha = 90°$ is smaller than that when $\alpha = 30°$ and 60°. As α keeps increasing, the adjacent ends of the two chiral particles carrying opposite electric charges are getting closer. This provides extra LC loads leading to the lower resonant frequency. On the other hand, increasing α makes the two ends of a single particle further, tending to increase the resonant frequency. These two effects both play a role in determining the resonant frequency, so there is no apparent difference between the two resonant frequencies when $\alpha = 90°$ and $\alpha = 130°$.

IV. Circular Polarizer Implementation

To convert a linearly polarized wave to a circularly polarized wave, a birefringent material is needed, such as the metasurface in [18]. Lack of any symmetry, our proposed 3-D chiral structure with large circular dichroism can be engineered to realize the linear-to-circular polarization conversion.

A. Simulations

The two pairs of aligned electric and magnetic dipoles in the proposed chiral particle cause the anisotropy of the chiral structure. Due to the anisotropy and highly tunable feature, the chiral structure can be designed for converting an x polarized wave to a circularly polarized wave. In this design, AD600 is chosen as the dielectric substrate. The relative permittivity and thickness are $\epsilon_r = 6.15$ and $h = 1.524$ mm. The loss tangent is 0.003. Segment lengths a and b are carefully optimized. The fina geometric parameters for the chiral particle in Fig. 1(c) and (d) are $a = 2.9$ mm, $b = 2.5$ mm, the radii of vias are 0.2 mm, and the width of line segments is 0.4 mm. $\alpha = 90°$ and the period of the unit cell is $p_x = 7$ mm and $p_y = 6$ mm. For experiments, we fabricate a chiral sample with 54×63 unit cells. The sample is shown in Fig. 1(a) and (b) and occupies an overall area of 378×378 mm^2.

The phase delay between the transmitted x- and y-components is adjusted based on two factors. First, arm lengths a and b. Similar to the twisting angle α, a and

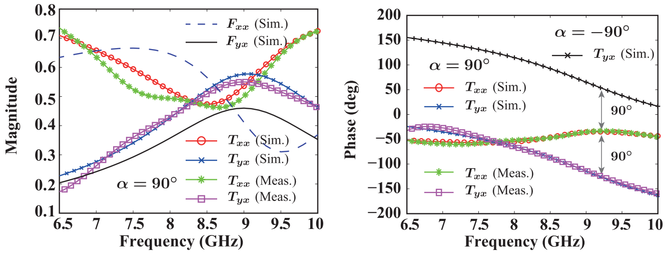

(a) (b)

Fig. 6. Simulation and/or experiment results of linear transmission and ref ection coeff cients for the chiral circular polarizer when it is illuminated by an x polarized wave. (a) Magnitude of transmission and ref ection coeff cients. (b) Phase of transmission coeffi ients.

b also infl ence the direction and strength of the induced electric and magnetic dipoles. Second, resonant frequency. The chiral anisotropy at off-resonant frequency is used to guarantee the desired retardation for the cross-polarized component as well as the same amplitude between the co- and cross-polarized components. Simulation and experiment results are shown in Fig. 6(a) and (b). Within the whole measured frequency band, a reasonable agreement between simulation and measurement results can be observed. At the operating frequency of 9.2 GHz, the magnitudes of T_{xx} and T_{yx} are equal to 0.565. With respect to the transmitted y component, the phase of the transmitted x-component is retarded by 90°, indicating a transmitted RCP wave. The efficie cy of a circular polarizer is determined by many factors, such as the substrate loss, copper loss, matching property, and undesired cross-polarized component. Compared to existing chiral polarizers, our proposed one has a great advantage that the phase delay between the transmitted x- and y-components is 90°, which attributes to the large chirality and high tunability. Therefore, there is no unwanted cross-polarized wave, i.e., the LCP one in this case. A portion of the incident wave is reflecte back due to the mismatch at the chiral slab and air interface. As can be found in Fig. 6(a), at the operating frequency, the total ref ected power occupies 33% of the total incident power. With the loss of the material counted, the remaining power completely goes into the RCP wave. From the experiment results, the conversion eff ciency of the chiral polarizer is about 64%. In contrast to conventional polarizers, the chiral polarizer has an ultra compact design. The size of the chiral unit cell at the operating frequency is approximated to be $0.21\lambda_0 \times 0.18\lambda_0$, where λ_0 is the incident wavelength.

Furthermore, based on previous descriptions, we can obtain a 180° phase shift for T_{yx} by simply switching the two arm orientations (twisting angle α is changed from 90° to −90°). Interestingly, the switched chiral polarizer can convert the x polarized wave to an LCP wave instead of RCP wave, as presented in Fig. 6(b).

B. Experiments

Measurements are implemented via a free-space EM transmission system. Two standard linear-polarized horn antennas working at the frequency ranging from 6.57 to 9.99 GHz are set as a transmitter and receiver, respectively, as shown in Fig. 7. A vector network analyzer is used to record and process

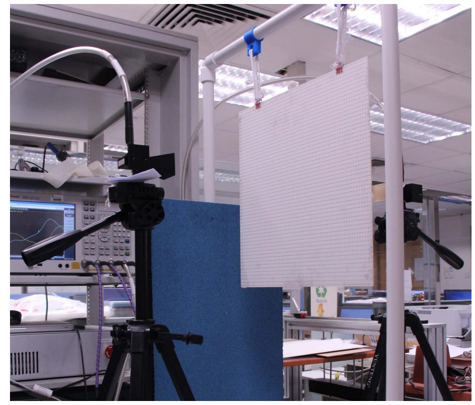

Fig. 7. Experimental setup for the transmission measurements of fabricated chiral samples.

time-domain transmitted signals. Since our horn antennas only emit and receive linearly polarized waves, transmission coef f cients in linear basis are obtained f rst. Circular transmission coefficient are then calculated based on the linear ones by (3).

For the measurement of co-transmission coefficient , two horn antennas need to be aligned and the EM response between them are calibrated. In our case, the distance between the two horn antennas is chosen to be around 60 cm to: 1) make sure the wave impinging on the sample is a plane wave; 2) avoid the edge/truction effect of the f nite periodic structures; 3) guarantee that suff cient unit cells are illuminated. Next, the sample is inserted between the two antennas. Cross-transmission coefficient are measured by rotating the receiving horn antenna by 90°.

During the experiment, a time-domain gate technique is employed to eliminate the disturbances from the mismatch of antennas and multiple reflecti ns between the antennas and sample. Gate parameters are fi st estimated with the distance from the sample to the receiver and transmitter. Then, the gate parameters are carefully tuned and chosen. After incorporating the time-domain gate, unwanted echoes are eliminated resulting in a smoother response in the frequency domain.

Measurement results are shown in Fig. 6. They are in good agreements with the simulation ones. The phase difference between T_{xx} and T_{yx} at the operating frequency is measured to be 90°; and magnitudes of both T_{xx} and T_{yx} are around 0.55. The measured magnitude is slightly lower than the simulated one, which is 0.565. It is reasonable due to the measurement error and imperfect material properties of substrate.

C. Comparisons

Another chiral sample with the same conf guration of the chiral circular polarizer except the twisting angle α (30°) is fabricated and measured for comparison.

During the measurement, we found that the measured data were inaccurate when the time-domain gate was applied, as plotted in Fig. 8(b). It is known that sharp changes in frequency domain imply a broadband time-domain response. To recover the sharp response of the sample around 7.2 GHz, time-domain information during a large time interval is needed. However, the desired time-domain gate avoiding the multiple reflecti ns also filte s out the useful information.

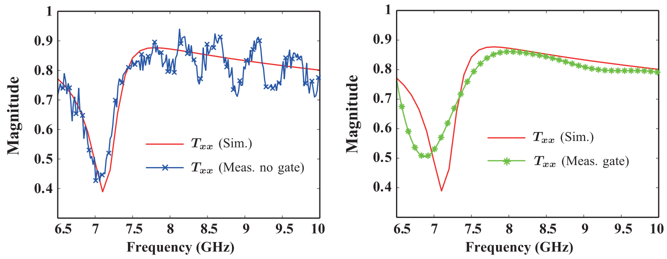

(a) (b)

Fig. 8. Simulation and experiment results of the alternate chiral sample ($\alpha = 30°$). (a) Simulation and measurement results without time-domain gate. (b) Simulation and measurement results with time-domain gate.

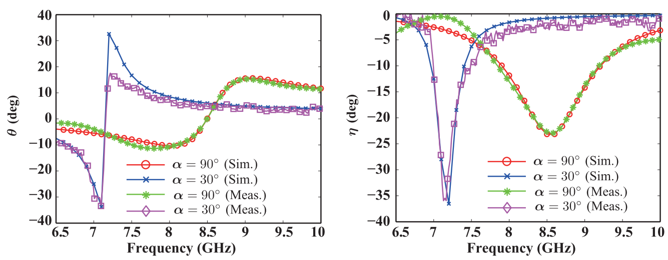

(a) (b)

Fig. 9. (a) Azimuthal rotation angle and (b) ellipticity of the chiral circular polarizer ($\alpha = 90°$) and the alternate chiral structure ($\alpha = 30°$).

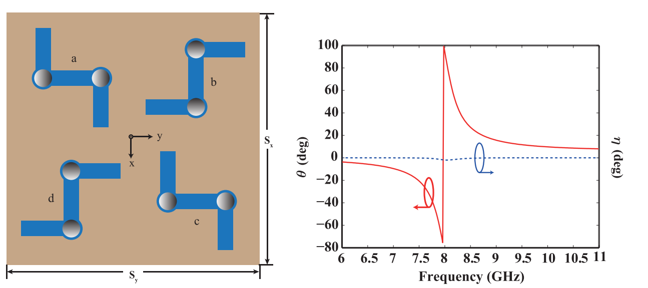

(a) (b)

Fig. 10. (a) Schematic of the uniaxial supercell. (b) Simulation results of the azimuthal rotation angle and ellipticity.

Truncation of this time-domain response will smoothen and broaden the tip in frequency domain, which is consistent with the results in Fig. 8(b). Trend of the measurement result without using a time-domain gate follows that of the simulated one well but ripples can be observed in Fig. 8(a).

Therefore, we abandon the time-domain gate during the measurement of the chiral sample with $\alpha = 30°$. Polarization responses of the sample with $\alpha = 30°$ and the chiral circular polarizer are examined and compared both numerically and experimentally. Azimuthal rotation angle θ and ellipticity η are plotted in Fig. 9. When $\alpha = 30°$, the peak values of both θ and η become larger. Good agreements can be observed between the simulation and experiment results. Effect of the signal multi-ref ection between antennas and the board when $\alpha = 30°$ can be found in the graph.

V. Supercell Arrangement

Until now, the chiral sample is sensitive to the polarization direction at normal incidence. We can achieve the isotropy under the normal incidence by arranging the chiral particle in C_4 symmetry (see Fig. 10). The four particles have the identical parameters as the chiral circular polarizer proposed in Section IV. The supercell is periodic along the x- and y-directions with the periodicity of 13×13 cm^2. The supercell size is $0.4\lambda_0 \times 0.4\lambda_0$ at 9.2 GHz. Therefore, it can be considered as a uniaxial structure. Besides the common features in C_4 symmetric structures, i.e., $T_{yx} = -T_{xy}$ and $T_{yy} = T_{xx}$, another feature can be found by the simulation results in Fig. 10(b). The ellipticity is very low with a maximum value of 2° around 8 GHz while the azimuthal rotation angle is 90°. Nearly a pure cross-linear polarized wave is generated at 8 GHz.

VI. Conclusion

In summary, to explore a strong polarization control capability, we proposed and systematically studied a 3-D omega-shaped chiral structure. The transmitted polarization states from the chiral structure are highly tunable, which is characterized by a large range of azimuthal rotation angle and ellipticity. Based on the proposed chiral particle, we also successfully realized a chiral circular polarizer, through which the linear polarized wave can be converted to the RCP or LCP wave. Experiment results show good agreements with the simulated ones. Finally, we developed a uniaxial chiral slab.

References

[1] J. A. Kong, *Electromagnetic Wave Theory*. Hoboken, NJ, USA: Wiley, 1986.

[2] J. B. Pendry, "A chiral route to negative refraction," *Science*, vol. 306, no. 5700, pp. 1353–1355, Nov. 2004.

[3] B. Wang, J. Zhou, T. Koschny, M. Kafesaki, and C. M. Soukoulis, "Chiral metamaterials: Simulations and experiments," *J. Opt. A, Pure Appl. Opt.*, vol. 11, no. 11, p. 114003, Sep. 2009.

[4] Z. Li, M. Mutlu, and E. Ozbay, "Chiral metamaterials: From optical activity and negative refractive index to asymmetric transmission," *J. Opt.*, vol. 15, no. 2, p. 023001, Jan. 2013.

[5] C. Menzel *et al.*, "Asymmetric transmission of linearly polarized light at optical metamaterials," *Phys. Rev. Lett.*, vol. 104, no. 25, p. 253902, Jun. 2010.

[6] R. Zhao, T. Koschny, and C. M. Soukoulis, "Chiral metamaterials: Retrieval of the effective parameters with and without substrate," *Opt. Exp.*, vol. 18, no. 14, pp. 14553–14567, 2010.

[7] E. Plum *et al.*, "Metamaterial with negative index due to chirality," *Phys. Rev. B*, vol. 79, no. 3, p. 035407, Jan. 2009.

[8] A. V. Rogacheva, V. A. Fedotov, A. S. Schwanecke, and N. I. Zheludev, "Giant gyrotropy due to electromagnetic-f eld coupling in a bilayered chiral structure," *Phys. Rev. Lett.*, vol. 97, no. 17, p. 177401, Oct. 2006.

[9] J. Zhou, J. Dong, B. Wang, T. Koschny, M. Kafesaki, and C. M. Soukoulis, "Negative refractive index due to chirality," *Phys. Rev. B*, vol. 79, no. 12, p. 121104(R), Mar. 2009.

[10] B. Wang, J. Zhou, T. Koschny, and C. M. Soukoulis, "Nonplanar chiral metamaterials with negative index," *Appl. Phys. Lett.*, vol. 94, no. 15, p. 151112, Apr. 2009.

[11] C. Rockstuhl, C. Menzel, T. Paul, and F. Lederer, "Optical activity in chiral media composed of three-dimensional metallic meta-atoms," *Phys. Rev. B*, vol. 79, no. 3, p. 035321, Jan. 2009.

[12] S. Zhang, Y.-S. Park, J. Li, X. Lu, W. Zhang, and X. Zhang, "Negative refractive index in chiral metamaterials," *Phys. Rev. Lett.*, vol. 102, no. 2, p. 023901, Jan. 2009.

[13] G. J. Molina-Cuberos, Á. J. García-Collado, I. Barba, and J. Margineda, "Chiral metamaterials with negative refractive index composed by an eight-cranks molecule," *IEEE Antennas Wireless Propag. Lett.*, vol. 10, pp. 1488–1490, 2011.

[14] Z. Li *et al.*, "Chiral metamaterials with negative refractive index based on four 'U' split ring resonators," *Appl. Phys. Lett.*, vol. 97, no. 8, p. 081901, Aug. 2010.

[15] M. Mutlu, A. E. Akosman, A. E. Serebryannikov, and E. Ozbay, "Asymmetric chiral metamaterial circular polarizer based on four U-shaped split ring resonators," *Opt. Lett.*, vol. 36, no. 9, pp. 1653–1655, May 2011.

[16] W. C. Chew, *Waves and Fields in Inhomogenous Media*. New York, NY, USA: IEEE Press, 1995.

[17] C. Menzel, C. Rockstuhl, and F. Lederer, “Advanced Jones calculus for the classif cation of periodic metamaterials,” *Phys. Rev. A*, vol. 82, p. 053811, Nov. 2010.

[18] H. F. Ma, G. Z. Wang, G. S. Kong, and T. J. Cui, “Broadband circular and linear polarization conversions realized by thin birefringent ref ective metasurfaces,” *Opt. Mater. Exp.*, vol. 4, no. 8, pp. 1717–1724, Aug. 2014.

Menglin L. N. Chen (S’14) received the B.Eng. degree from the University of Birmingham, Birmingham, U.K., the B.S. degree from the Huazhong University of Science and Technology, Wuhan, China, in 2012, and the M.S. degree from the University of Hong Kong, Hong Kong, in 2013, all in electronic engineering. She is currently pursuing the Ph.D. degree with the Electromagnetics and Optics Research Laboratory, Department of Electrical and Electronic Engineering, University of Hong Kong.

She was a Research Assistant with the Department of Electrical and Electronic Engineering, University of Hong Kong, from 2013 to 2014. Her current research interests include antenna design and metamaterials.

Li Jun Jiang (S’01–M’04–SM’13) received the B.S. degree in electrical engineering from Beihang University, Beijing, China, in 1993, the M.S. degree from Tsinghua University, Beijing, in 1996, and the Ph.D. degree from the University of Illinois at Urbana–Champaign, Champaign, IL, USA, in 2004.

He was an Application Engineer with the Hewlett-Packard Company, Palo Alto, CA, USA, from 1996 to 1999. Since 2004, he has been a Post-Doctoral Researcher, Research Staff Member, and Senior Engineer at the IBM T. J. Watson Research Center, Yorktown Heights, NY, USA. Since 2009, he has been an Associate Professor with the Department of Electrical and Electronic Engineering, University of Hong Kong, Hong Kong. From 2014 to 2015, he was a Visiting Scholar with the University of California at Los Angeles, Los Angeles, CA, USA. His current research interests include electromagnetics, computational electromagnetics, IC signal/power integrity, IC electromagnetic compatibility/electromagnetic interference, antennas, and multiphysics modeling.

Dr. Jiang has been an elected TPC Member of the IEEE EPEP since 2014, TPC Member of the IEEE EDAPS since 2010, TPC Member of the 2013 IEEE ICMTCE, Scientif c Committee Member of the 2010 IEEE SMEE, the Special Session Organizer of the IEEE EDAPS, the IEEE EMC, the ACES, the AP-RASC, the PIERS, the Co-Organizer of the HKU Computational Science and Engineering Workshops in 2010-2012, TC-9 and TC-10 Member of the IEEE EMC-S since 2011, and the Session Chair of many international conferences. He was a recipient of the HP STAR Award in 1998, the IEEE MTT Graduate Fellowship Award in 2003, the Y. T. Lo Outstanding Research Award in 2004, and the IBM Research Technical Achievement Award in 2008. He is the Associate Editor of the IEEE TRANSACTIONS ON ANTENNAS AND PROPAGATION, the Editor of *Progress in Electromagnetics Research*, the Associate Editor of *ACES Express*, and the Associate Guest Editor of the PROCEEDINGS OF THE IEEE Special Issue in 2011 and 2012. He is an IEEE AP-S Member, an IEEE MTT-S Member, an ACES Member, and a member of Chinese Computational Electromagnetics Society. His research team has received First Place for the Best Student Paper Award at the 2013 IEEE 14th HK AP/MTT Postgraduate Conference in AP Session, Second Place for the Best Student Paper Award at the 2013 IEEE 14th HK AP/MTT Postgraduate Conference in MTT Session, the Best Student Paper Award at the 2014 ACES, Florida, the Student Paper Award at the 12th International Workshop on Finite Elements for Microwave Engineering in 2014, and the Best Oral Paper Award at the 2014 IEEE EPEP Conference at Portland, Oregon. He is the TPC Chair of the 2016 IEEE APEMC, the 7th International Conference on Nanophotonics (ICNP)/the 3rd Conference on Advances in Optoelectronics and Micro/Nano Optics, and the CEM of 2015-2016 PIERS, the TPC Co-Chair of the 12th International Workshop on Finite Elements for Microwave Engineering, the Co-Chair of the 2013 International Workshop on Pulsed Electromagnetic Field at Delft, the Netherlands, and the General Chair of the 2014 IEEE 14th HK AP/MTT Postgraduate Conference. He also serves as a Reviewer for the IEEE TRANSACTIONS on several topics, and other primary electromagnetics and microwave-related journals.

Wei E. I. Sha (M’08) received the B.S. and Ph.D. degrees in electronic engineering from Anhui University, Hefei, China, in 2003 and 2008, respectively.

He was a Post-Doctoral Research Fellow with the Department of Electrical and Electronic Engineering, University of Hong Kong, Hong Kong, from 2008 to 2012, where he is currently a Research Assistant Professor. He has co-authored two books on wavelet theory and the f nite-difference time-domain method. He has authored 70 peer-reviewed journal papers included in the Web of Science Core Collection. He has also contributed to four book chapters at Springer, CRC Press, and InTech Publishers. He is involved in theoretical and computational research in electromagnetics and optics, focusing on multiphysics and interdisciplinary research. His research topics are inspired by applications in several areas including solar energy, microwave/optical communication, sensing/detection, and quantum information. His current research interests include fundamental and applied aspects in plasmonics, emerging photovoltaics, metasurfaces, quantum electrodynamics, and computational electromagnetics.

Dr. Sha is an OSA Member. He has served as a Committee Member or the Session Chair of several international conferences, including PIERS 2016, ICCEM 2016, IMWS-AMP 2015, EICT 2015, and ICSPS 2011. He received the Second Prize and the First Prize in the National Postgraduates Mathematical Contest in Modeling, in 2006 and 2007, respectively. He was a recipient of the Chinese Youth Science and Technology Innovation Prize in 2007. In 2015, he was a recipient of Second Prize of Natural Science from Anhui Province Government. He and his students received the Second Place for the Best Student Paper at PIERS 2014, First Place for the Best Student Paper at ACES 2014, and the Best Student Paper at NCMMW 2015. In 2014, he was awarded Outstanding Reviewer of the *Journal of Computational Physics*. He and his collaborators received the Research Output Prize at the University of Hong Kong in 2013. He has been serving as a Reviewer for the IEEE, OSA, AIP, APS, and Nature Publishing Group journals. He has also served as the Book Proposal Reviewer for CRC Press and Bentham Science.

Wallace C. H. Choy (SM’07) received the Ph.D. degree in electronic engineering from the University of Surrey, Guildford, U.K., in 1999.

He is currently a Professor in the Department of Electrical and Electronic Engineering, University of Hong Kong, Hong Kong, after vigorous working experience with the National Research Council of Canada, Ottawa, ON, Canada, and Fujitsu, San Jose, CA, USA, on investigating optoelectronic devices. He has been recognized as the Top 1% of the most-cited scientists in Thomson Reuter’s Essential Science Indicators in 2014 and 2015. He has authored over 160 internationally peer-reviewed journal papers, contributed to seven book chapters, holds four U.S. and Chinese patents, and edited one book published by Springer. His current research interests include organic/inorganic optoelectronic devices, plasmonic structures, nanomaterial and nonlinear optical devices, and physics.

Prof. Choy has served as an Editorial Board Member for the Nature Publishing Group of *Scientific Reports* and IOP *J Physics D*, Topical Editor of the OSA *Journal of the Optical Society of America B* (JOSA was founded in 1917), and and Associate Editor of the IEEE PHOTONIC JOURNALS, and Guest Editor of the OSA *Journal of Photonic Research* and *Journal of Optical Quantum Electronics*.

Tatsuo Itoh (S'69–M'69–SM'74–F'82–LF'06) received the Ph.D. degree in electrical engineering from the University of Illinois at Urbana–Champaign, Champaign, IL, USA, in 1969.

He was with the University of Illinois at Urbana–Champaign, Stanford Research Institute, Menlo Park, CA, USA, and the University of Kentucky, Lexington, KY, USA. He joined the faculty of the University of Texas at Austin, Austin, TX, USA, in 1978, where he became a Professor of Electrical Engineering in 1981, and where, in 1983, he was selected to hold the Hayden Head Centennial Professorship of Engineering. In 1991, he joined the University of California at Los Angeles, Los Angeles, CA, USA, as a Professor of Electrical Engineering and holder of the Northrop Grumman Endowed Chair in Microwave and Millimeter-Wave Electronics. He has authored 440 journal publications, 880 refereed conference presentations, and 48 books/book chapters in the area of microwaves, millimeter-waves, antennas, and numerical electromagnetics. He supervised 80 Ph.D. students.

Dr. Itoh was a recipient of a number of awards, including the IEEE Third Millennium Medal and the IEEE MTT Distinguished Educator Award in 2000, the Outstanding Career Award from the European Microwave Association in 2009, the Microwave Career Award from the IEEE MTT Society in 2011, and the Alumni Award for Distinguished Service from the College of Engineering, University of Illinois at Urbana–Champaign, in 2012. He is a member of the Institute of Electronics and Communication Engineers of Japan and Commissions B and D of USNC/URSI. He was elected as an Honorary Life Member of the MTT Society in 1994 and a member of the National Academy of Engineering in 2003. He was the President of the Microwave Theory and Techniques Society in 1990 and Chairman of Commission D of the International URSI from 1993 to 1996. He served as the Distinguished Microwave Lecturer in Microwave Applications of Metamaterial Structures of the IEEE MTT-S in 2004 and 2006. He serves on the Advisory Boards and Committees of a number of organizations. He was the Editor of the IEEE TRANSACTIONS ON MICROWAVE THEORY AND TECHNIQUES from 1983 to 1985, and the Editor-in-Chief of the *IEEE Microwave and Guided Wave Letters* from 1991 to 1994.